Finite element modeling of nanoindentation on an elastic-plastic microsphere

Jialian Chen
Fujian Normal University
Hongzhou Li (lihongzhou@fjnu.edu.cn)
Fujian Normal University https://orcid.org/0000-0001-8005-1323

Original Article

Keywords: Microsphere, Finite element analysis, Nanoindentation, Plasticity, Mechanical properties

Posted Date: May 7th, 2020

DOI: https://doi.org/10.21203/rs.3.rs-25785/v1

Finite element modeling of nanoindentation on an elastic-plastic microsphere

Jialian Chen[a], Hongzhou Li[a, b, *]

[a]College of Environmental Science and Engineering, Fujian Normal University, Fuzhou 350007, Fujian, China

[b]Engineering Research Center of Polymer Resources Green Recycling of Ministry of Education, Fujian Normal University, Fuzhou 350007, Fujian, China

Corresponding author. Tel.: +86 591 83426504; Fax: +86 591 83465225.

E-mail address: lihongzhou@fjnu.edu.cn (H. Li).

Abstract

The understanding of the mechanical indentation on a curved specimen (e.g., microspheres and microfibers) is of paramount importance in the characterization of curved micro-structured materials, but there has been no reliable theoretical method to evaluate the mechanical behavior of nanoindentation on a microsphere. This article reports a computational study on the instrumented nanoindentation of elastic-plastic microsphere materials via finite element simulation. The finite element analyses indicate that all loading curves are parabolic curves and the loading curve for different materials can be calculated from one single indentation. The results demonstrate that the Oliver-Pharr formula is unsuitable for calculating the elastic modulus of nanoindentation involving cured surfaces. The surface of the test specimen of a microsphere requires prepolishing to achieve accurate results of indentation on a micro-spherical material. This study provides new insight into the establishment of nanoindentation models that can effectively be used to simulate the mechanical behavior of a microsphere.

Keywords: Microsphere; Finite element analysis; Nanoindentation; Plasticity; Mechanical properties

1. Introduction

Instrumented nanoindentation is perhaps the most commonly adopted and used technique in the characterization of mechanical behavior of microplastics, thin films, coatings, powders, small crystals and materials at small scales. One of the great advantages of the technique is that many mechanical properties of materials can be determined by the analyses of indentation load-displacement data alone, thereby avoiding the need to measure the area of hardness impression by imaging and facilitating property measurement at the sub-micron scale [1, 2]. In a nanoindentation test, an axisymmetric diamond indenter with a geometry known to high precision (usually a Berkovich tip, which has three-sided pyramid geometry with the same area-to-depth ratio as the four-sided Vickers pyramid used commonly in microhardness testing) is pushed into the surface of test specimen with an increased force or displacement. As the force or displacement reaches a user-defined maximum value (sometimes moving just a few hundreds of atom into solid surface, indentation depth 20 or 30 nanometers), the load is then withdrawn. While loading-unloading is in progress, force-displacement curves are recorded via a Nanoindenter® instrument. The unloading curve is used to extract the mechanical properties (including elastic modulus and hardness) of test specimen via an analytical method, such as the Oliver-Pharr method [3, 4]. For Oliver-Pharr method, the test specimen is assumed to be a flat surface with linear isotropic elastic-perfectly plastic material properties. A permanent hardness impression is formed during loading and unloading. When the indenter is unloaded, the elastic strains are recovered. Thus, instrumented nanoindentation has elastic and plastic deformation during loading, but only elastic deformation during unloading.

Cheng and Cheng derived several scaling relationships for conical indentation in elastic-plastic solids with work hardening using dimensional analysis and finite element calculations [5]. They pointed out that some properties such as the elastic modulus are size independent [6]. The measured

values from macroscopic experiments are consistent with that predicted from first-principles quantum mechanics calculations. Oliver and Pharr reviewed the mechanics governing elastic-plastic indentation as they pertain to load and depth-sensing indentation testing of monolithic materials [7]. The measurement of contact stiffness by dynamic techniques allows for continuous measurement of properties as a function of depth. Stiffness is measured continuously during the loading of the indenter by imposing a small dynamic oscillation on the force (or displacement) signal and measuring the amplitude and phase of the corresponding displacement (or force) signal by means of a frequency-specific amplifier [7]. The elastic and plastic properties of materials by employing instrumented sharp (geometrically self-similar indenters like Vickers, Pyramids, Berkovich or Cones) indentation may be computed from a single loading-displacement curve through a general theoretical framework proposed by Giannakopoulos and Suresh [8]. Their procedure can be used to accurately predict the indentation response from a given set of elastic-plastic properties (forward algorithms), and to extract elastic-plastic properties from a given set of indentation data (reverse algorithms) [9]. Pileup (or sink-in) leads to contact areas that are greater than (or less than) the cross-sectional area of the indenter at a given depth. These effects lead to errors in the absolute measurement of mechanical properties by nanoindentation. The measured indentation modulus and hardness would be too high in the case of pileup and too low in the case of sink-in without accounting for the difference between the actual contact area and the cross-sectional area of the indenter [10]. Saha and Nix examined the effects of substrate on determining the mechanical properties of thin films by nanoindentation [11]. Compared to hardness, the nanoindentation measurement of the elastic modulus of thin films is more strongly affected by substrate. True contact area and true hardness of film can be determined from the measured contact stiffness, irrespective of the effects of pileup or sink-in around the indenter.

Much research has been done on the indentation problem of a half-space by a rigid indenter [12-14]. However, not all small scale structures are flat. Examples of small scale microplastics and fibers

(typical diameter 10-20um) require material characterization. The material properties are not affected by the geometry of the test specimen, but the Oliver-Pharr procedure to obtain material properties will vary according to the geometry of the testing specimen. There has been no reliable theoretical method to evaluate the mechanical behavior of nanoindentation on a curved specimen. It is necessary to conduct reliable numerical simulations to evaluate the mechanical behavior of nanoindentation on a microsphere. The numerical simulations are usually carried out via the finite element method [15-30]. Phadikar and Karlsson investigated the possibility of extending instrumented indentation to non-flat surfaces [21-22, 27-29]. In this study, finite element method had been used to systematically investigate the mechanical behavior of nanoindentation on a microsphere.

2. Theoretical Background

The analysis of Sneddon for the indentation of an elastic half space by a flat, cylindrical punch leads to a simple relation between P and h of the form [31]

$$P=\frac{4Ga}{1-\nu}h \qquad (1)$$

where P is the indenter load, h is the displacement of the indenter relative to the initial undeformed surface, a is the radius of the cylinder, G is shear modulus, and ν is Poisson's ratio of testing specimen. Noting that the contact area A is equal to πa^2 (i.e., the projected area or cross sectional area of elastic contact) and that shear modulus is equal to $E/[2(1+\nu)]$, differentiating P with respect to h leads to

$$S=\frac{dP}{dh}=\frac{2E\sqrt{A}}{(1-\nu^2)\sqrt{\pi}} \qquad (2)$$

where $S=dP/dh$ is the initial stiffness of the unloading curve, defined as the slope of the upper portion of the unloading curve during the initial stages of unloading (also called contact stiffness), and E is the Young's modulus of testing specimen. For the Berkovich and Vickers pyramids, the

equivalent cone angle is 70.296°, and the area-to-depth relationship, also known as the area function, is given by

$$A = 24.494 h_c^2 \qquad (3)$$

where A is the cross-sectional area of the indenter at a distance h_c (contact depth) back from its tip. Known the contact depth, and the shape of the indenter determined through the "area function", the contact area is then determined. If the contact stiffness and contact area were known, Equation 2 and Equation 3 can be used to measure the elastic modulus of a material. Taking one complete cycle of loading and unloading data, three quantities are measured: one is the maximum load, another is the maximum displacement h_{max} (the maximum displacement of the indenter relative to the initial undeformed surface), and the third is the unloading stiffness.

Effects of non-rigid indenters on the load-displacement behavior can be effectively accounted for by defining an effective elastic modulus through the equation [4]

$$\frac{1}{E_{eff}} = \frac{(1-\nu^2)}{E} + \frac{(1-\nu_i^2)}{E_i} \qquad (4)$$

where E_i and ν_i are the Young's modulus and Poisson's ratio of the indenter. If the indenter is a rigid body (i.e., $E_i = \infty$), for any axisymmetric indenter, the effective elastic modulus E_{eff} can be derived as [4]

$$E_{eff} = \frac{\sqrt{\pi}}{2}\frac{S}{\sqrt{A}} \qquad (5)$$

If the indenter is a conical indenter, then

$$E = E_{eff}(1-\nu^2) = \frac{\sqrt{\pi}}{2}\frac{S}{\sqrt{A}}(1-\nu^2) \qquad (6)$$

The normal definition of hardness H is

$$H = \frac{P_{max}}{A} \qquad (7)$$

where P_{max} is the peak indentation load.

The Young's modulus and hardness extracted from the Oliver-Pharr method are dependent on the initial stiffness of the unloading curve and the projected area of the indentation at the contact depth h_c. To correct Oliver-Pharr's solution accounting for the radial displacements, Hay used finite element method to calibrate Equation 2 and included a "correction factor" [32]. The correction factor is dependent on the half-included angle of indenter and Poisson's ratio of a material

$$S = \gamma \frac{2E_{OP}\sqrt{A}}{(1-\nu^2)\sqrt{\pi}} \qquad (8)$$

where γ is the correction factor, and E_{OP} is the Young's modulus extracted according to Oliver-Pharr method. The correction factor appearing in Equation 8 plays a very important role when accurate property measurements are desired. This constant affects the elastic modulus calculated from the contact stiffness by means of Equation 8 because procedures for determining the indenter area function are also based on Equation 8. Oliver and Pharr proposed that $\gamma = 1.05$ with a potential error of approximately ±0.05, based on their analysis of available results $1.0226 \le \gamma \le 1.085$ from experiments and finite element calculations [7].

3. Finite element Model

To reduce testing, finite element analysis is used to calculate the load-displacement curves of nanoindentation during the loading and unloading, and the unloading curve can be used to determine the Young's modulus of a material using the Oliver-Pharr method (reverse algorithms). Finite element analyses of nanoindentation tests were carried out on an elastic-plastic microsphere. Figure 1a shows the finite element model of a microsphere with 11.5μm radius and the mesh generated using ABAQUS, in which two dimensional CAX4R (continuum, axisymmetric, quadrilateral four-node reduced integration) and CAX3 elements were used in the mesh discretization of the microsphere. The whole model consists of 28651 elements and 28538 nodes. A finer mesh near the contact region and a

gradually coarser mesh further from the contact region were designed to ensure numerical accuracy (Figure 1b). The mesh was well tested for convergence and was determined to be insensitive to far-field boundary conditions. Based on symmetry, only one half of the microsphere is modeled. The lower half surface of the half microsphere is fixed in all directions. A rigid Berkovich indenter of semi apex angle 70.296° was employed on the top of the half microsphere. The indentation is displacement controlled by imposing a vertical displacement on the rigid Berkovich indenter. The selection of proper incremental step size is important due to the highly nonlinear nature of the problem, which involves nonlinear material properties, nonlinear geometry and contact between one pair of surfaces. The friction coefficient for the contact elements between the indenter and the half microsphere was set to be zero.

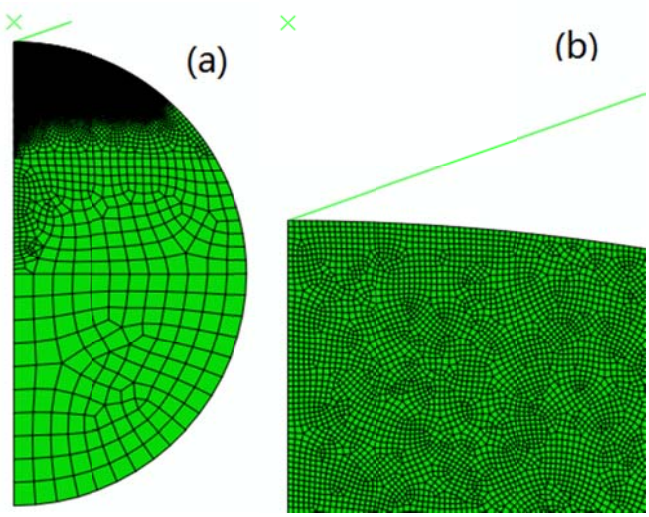

Figure 1 Finite element mesh: (a) one half of a microsphere, (b) enlargement of refined mesh at the vicinity of Berkovich indenter

4. Results and Discussion

Dimensional analysis is widely used as a guideline for evaluating indentation testing and is used here. Yan established a set of non-dimensional relations for conical indentation on a homogeneous, isotropic semi-infinite flat substrate including quantity E/σ_y [17]. σ_y is the initial yield stress of linear-elastic,

perfectly-plastic material. σ_y / E is initial yield strain. Phadikar showed that $h_{\max} / \mathrm{R}$ (R is the radius of the microsphere) is an appropriate non-dimensional factor [21]. Therefore, we selected E / σ_y and $h_{\max} / \mathrm{R}$ quantities to present our results. In order to research the effect of E / σ_y on indentation, the Young's modulus and the Poisson's ratio of the microsphere was set to be 10GPa and 0.2, respectively. The ratio of Young's modulus of the microsphere over the initial yield stress of the microsphere, E / σ_y, was systematically varied between 10 and 1000 to cover the most mechanical properties of materials encountered in engineering. An elastic–plastic material with $E / \sigma_y = 70$ is fairly typical for a polymer (low-density polyethylene with $E = 1.37\mathrm{GP}a$, $\sigma_y = 20\mathrm{MPa}$, $E / \sigma_y \approx 69$; aluminum with $E = 70\mathrm{GP}a$, $\sigma_y = 228\mathrm{MPa}$, $E / \sigma_y \approx 307$).

Figure 2 shows that microsphere is penetrated with different indentation depths via the rigid Berkovich indenter to produce different maximum loads. All the loading curves at different indentation depths overlap and follow exactly the same loading curve. The load is proportional to the square of the indenter displacement during loading as $P = \dfrac{2E \tan \phi}{\pi(1-\nu^2)} h^2$, where ϕ is the half-included angle of indenter. Therefore, the indentation curves exhibit parabolic loading and power-law unloading. The residual depth after full unloading is larger for deeper indentation. The area under the loading curve is the total work; the area under the unloading curve is the reversible work; and the area enclosed by the loading and unloading curve is the irreversible work. The total work and the reversible work are proportional to the maximum depth $h_{\max}^3$.

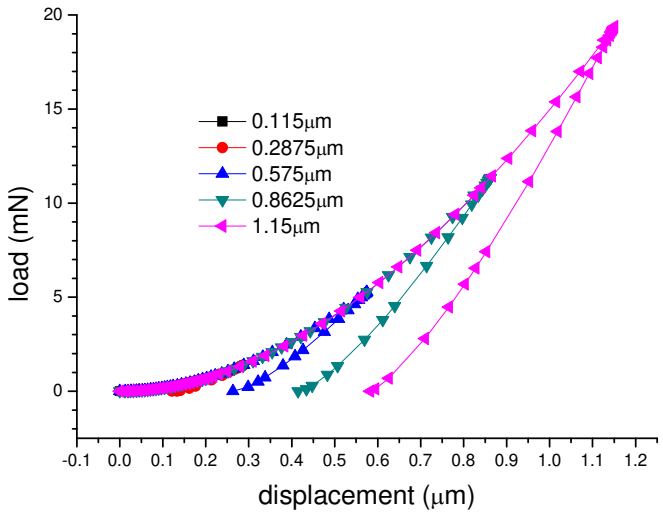

Figure 2 Loading and unloading curves for different indentation depths of $E/\sigma_y = 10$

Figure 3a shows the loading and unloading curves for different E/σ_y at indentation depth 0.115μm. As shown in Figure 3a, the indenter displacement in $E/\sigma_y = 200-1000$ is plastic, and only a small portion of elasticity is recovered on unloading. The surface around the indenter piles up. However, the indenter displacement in $E/\sigma_y = 10-50$ is more elastic, a larger portion of elasticity is recovered on unloading. The surface around the indenter sinks in. For highly elastic solids, such as polymers, sink-in is often observed. $E/\sigma_y = 100$ is a critical value for surface pileup or sink-in for this case. The surface near the indenter has a tendency to pile up around the indenter and forms a "crater" when E/σ_y is greater than 100. However, when E/σ_y is less than 100, the surface near the indenter sinks in. The load of each curve in Figure 3b is normalized with respect to its maximum load in Figure 3a, respectively. As shown in Figure 3b, all loading curves overlap. It means that all loading curves in Figure 3a are proportional for different E/σ_y. It means that all loading curves for different materials can be calculated from one single indentation.

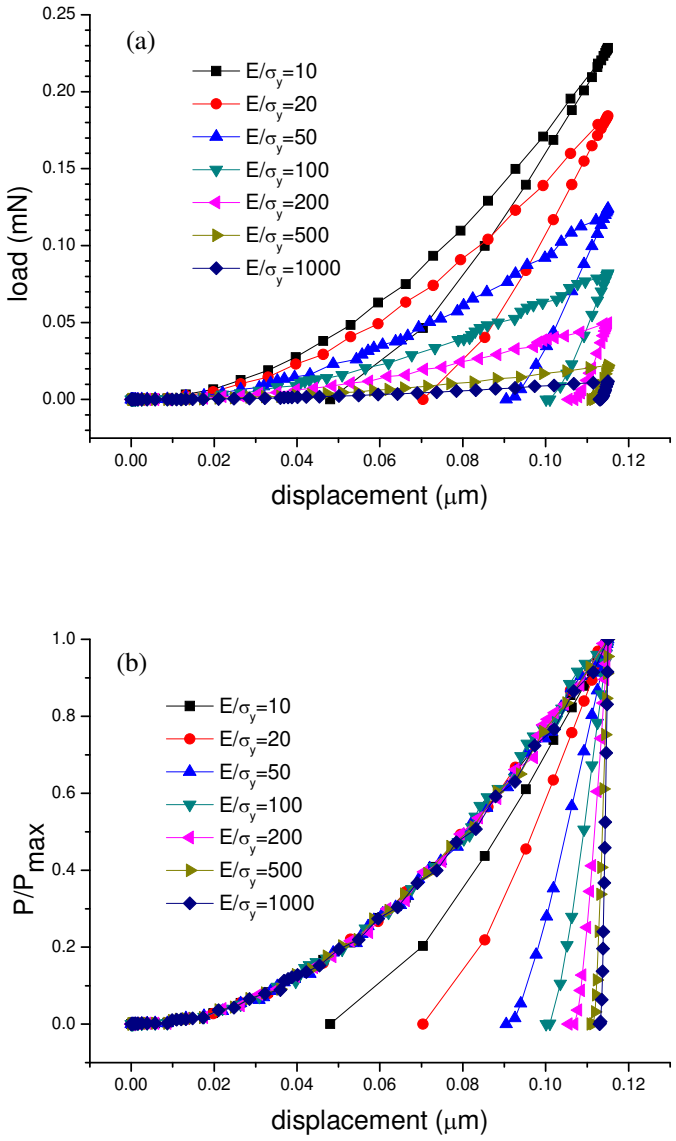

Figure 3 Loading and unloading curves for different E/σ_y at indentation depth 0.115μm: (a) original curves, (b) curves normalized by maximum load

Figure 4a shows the input Young's modulus in the finite element code normalized with respect to Young's modulus extracted according to the Oliver-Pharr method, E/E_{OP}, as a function of normalized maximum indentation depth, h_{max}/R. The initial unloading slope was computed using the two points associated with the maximum load and 1% of the unloading curve as shown in Figure 2 and Figure 3a.

Then, the Oliver-Pharr modulus E_{OP} can be obtained according to Equation 2. The values $E/E_{OP}=\gamma=\sqrt{\frac{24.494}{\pi}}\frac{2E}{(1-\nu^2)}\frac{h_c}{S}$ in Figure 4 correspond to the "correction factor" extracted from the Oliver-Pharr method. The correction factor is not a constant with the increase of normalized maximum indentation depth even for the same E/σ_y. This means that the calculated elastic modulus of a microsphere using the Oliver-Pharr method according to simulated unloading curve is dependent on the indentation depth. As a consequence, suggesting that formula 2 is unsuitable for calculating the elastic modulus of nanoindentation involving cured surfaces. The surface of the test specimen of a microsphere requires prepolishing to achieve accurate results of indentation on a microsphere material. Figure 4b shows that as long as the ratio of Young's modulus of the microsphere over the initial yield stress of the microsphere, E/σ_y, is the same value, the calculated E/E_{OP} is equal for the same indentation depth. It substantiates that Young's modulus can be normalized with yield stress as a non-dimensional quantity E/σ_y.

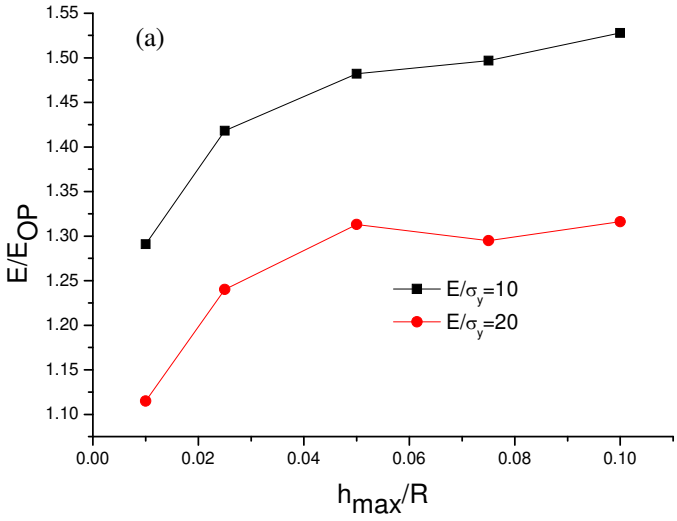

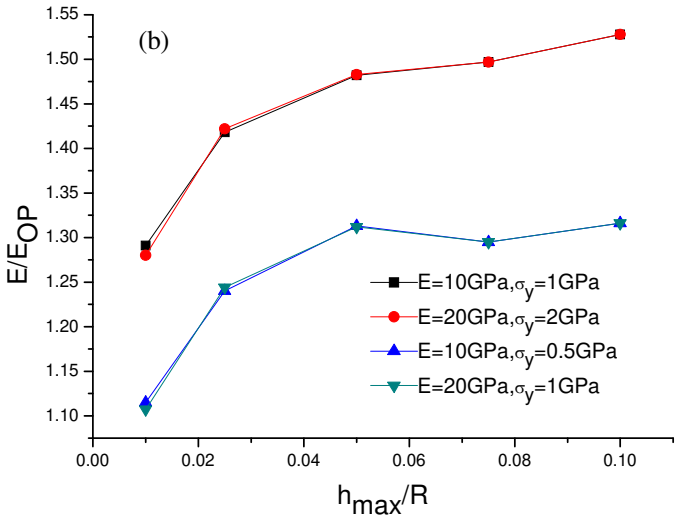

Figure 4 Normalized Young's modulus E/E_{OP} as a function of maximum indentation depth over microsphere radius: (a) vary σ_y, (b) vary E

Figure 5 shows the final depth h_f (the residual depth relative to the initial undeformed surface) as a function of the ratio of maximum indentation depth over microsphere radius h_{max}/R. The final depth increases with the increase of E/σ_y and h_{max}/R. Figure 6 shows the loading and unloading curves for $E/\sigma_y = 10$ and $E/\sigma_y = 20$ at indentation depth 0.115μm. It clearly shows that the final depths after indentation are equal for the same E/σ_y.

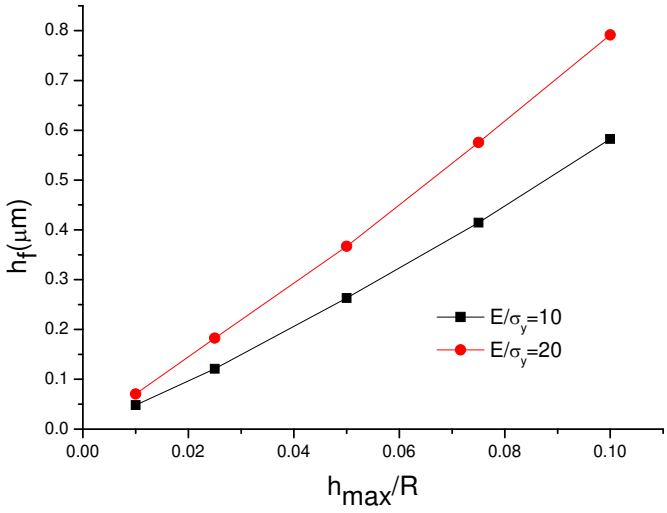

Figure 5 Final depth as a function of maximum indentation depth over microsphere radius

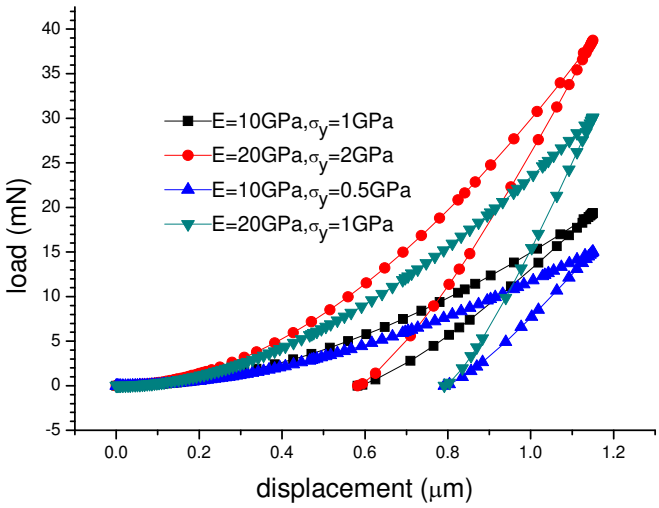

Figure 6 Loading and unloading curves for $E/\sigma_y = 10$ and $E/\sigma_y = 20$ at indentation depth 0.115μm

The stress distribution inside the microsphere at any time during indentation, the residual stress distribution inside the microsphere, the permanent deformation of the microsphere can be predicted via finite element analyses. Figure 7 shows the stress fields at maximum indentation force, the permanent deformation and residual stress distributions inside the microsphere after full unloading. In the purely

elastic contact solution, material always sinks in, while for elastic-plastic contact, material may either sink in or pile up. The fundamental material properties affecting pileup are the ratio of the effective modulus to the yield stress E/σ_y. In general, pileup is greatest in materials with the large E/σ_y ratios, such as soft materials. Hard materials and most polymers, ceramics, and glasses have small E/σ_y ratios. As E/σ_y decreases, corresponding to increases in the yield stress and decreases in h_f/h_{max}, the size of the plastic zone decreases until, at some point, the plastic zone boundary in the surface coincides with the contact perimeter indicating the transition from pileup to sink-in behavior. It indicates that whether a non-work hardening material piles up or sinks in during nanoindentation has correlation to the size of plastic zone as shown in Figure 7.

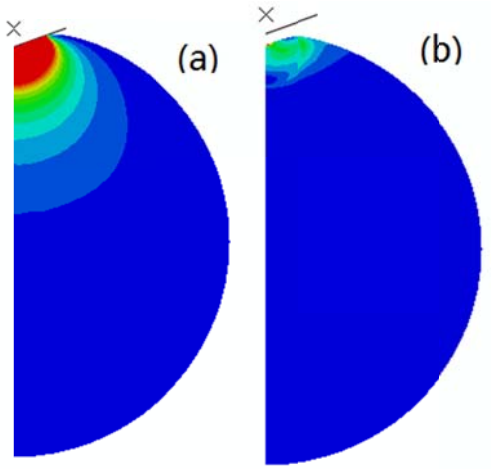

Figure 7 Stress distribution inside microsphere for indentation depth 1.15μm of $E/\sigma_y = 10$: (a) at maximum loading, (b) after full unloading

5. Conclusion

A computational study was undertaken to simulate the instrumented nanoindentation of elastic-plastic microsphere materials. The ratio of Young's modulus of the microsphere over the initial yield stress of the microsphere, E/σ_y, was systematically varied from 10 to 1000 to cover the most mechanical properties of materials encountered in engineering. Finite element simulation results indicate that the load is proportional to the square of the indenter displacement during loading as $P = \frac{2E\tan\phi}{\pi(1-\nu^2)}h^2$. The total work and the reversible work are proportional to the maximum depth $h_{\max}^3$. The calculated elastic modulus of a microsphere using Oliver-Pharr formula according to simulated unloading curve was found to be dependent on the indentation depth, suggesting that this formula is unsuitable for calculating the elastic modulus of nanoindentation involving cured surfaces. The surface of the test specimen of a microsphere requires prepolishing to achieve accurate results of indentation on a micro-spherical material.

Acknowledgments

We want to thank professors Aette M. Karlsson and John W. Gillespie for help with the research design. Furthermore, we want to thank the editor and the anonymous reviewers for valuable and helpful comments on the manuscript.

Funding

This work was supported by the Fujian Provincial Department of Science and Technology (2018Y4002) and the National Natural Science Foundation of China (51103173).

Authors' contributions

J.L. Chen revised the manuscript. H.Z. Li contributed to research design, calculations, analysis and interpretation of results, and writing of the manuscript.

Competing interests

The authors declare that they have no competing interests.

Availability of data and materials

All data needed to evaluate the conclusions in the paper are present in the paper. Additional data related to this paper may be requested from the corresponding author.

References

1. Pharr GM. Measurement of mechanical properties by ultra-low load indentation. Materials Science and Engineering A-Structural Materials Properties Microstructure and Processing, 1998, 253(1-2): 151-159.
2. Bolshakov A, Pharr GM. Influences of pileup on the measurement of mechanical properties by load and depth sensing indentation techniques. Journal of Materials Research, 1998, 13(4): 1049-1058.
3. Oliver WC, Pharr GM. An improved technique for determining hardness and elastic modulus using load and displacement sensing indentation experiments. Journal of Materials Research, 1992, 7(6): 1564-1583.
4. Pharr GM, Oliver WC, Brotzen FR. On the generality of the relationship among contact stiffness, contact area, and elastic modulus during indentation. Journal of Materials Research, 1992, 7(3): 613-617.
5. Cheng YT, Cheng CM. Scaling approach to conical indentation in elastic-plastic solids with work

hardening. Journal of Applied Physics, 1998, 84(3): 1284-1291.

6. Cheng YT, Cheng CM. Scaling, dimensional analysis, and indentation measurements. Materials Science & Engineering R-Reports, 2004, 44(4-5): 91-149.
7. Oliver WC, Pharr GM. Measurement of hardness and elastic modulus by instrumented indentation: Advances in understanding and refinements to methodology. Journal of Materials Research, 2004, 19(1): 3-20.
8. Giannakopoulos AE, Suresh S. Determination of elastoplastic properties by instrumented sharp indentation. Scripta Materialia, 1999, 40(10): 1191-1198.
9. Dao M, Chollacoop N, Van Vliet KJ, Venkatesh TA, Suresh S. Computational modeling of the forward and reverse problems in instrumented sharp indentation. Acta Materialia, 2001, 49(19): 3899-3918.
10. McElhaney KW, Vlassak JJ, Nix WD. Determination of indenter tip geometry and indentation contact area for depth-sensing indentation experiments. Journal of Materials Research, 1998, 13(5): 1300-1306.
11. Saha R, Nix WD. Effects of the substrate on the determination of thin film mechanical properties by nanoindentation. Acta Materialia, 2002, 50(1): 23-38.
12. Kogut L, Etsion I. Elastic-plastic contact analysis of a sphere and a rigid flat. Journal of Applied Mechanics-Transactions of the ASME, 2002, 69(5): 657-662.
13. Zhao MH, Chen X, Yan J, Karlsson AM. Determination of uniaxial residual stress and mechanical properties by instrumented indentation. Acta Materialia, 2006, 54(10): 2823-2832.
14. Tong L, Liu G. Nanoscale reciprocating sliding contacts of textured surfaces: influence of structure parameters and indentation depth. Chinese journal of mechanical engineering, 2018, 31(1): 62.
15. Chen X, Vlassak JJ. Numerical study on the measurement of thin film mechanical properties by means of nanoindentation. Journal of Materials Research, 2001, 16(10): 2974-2982.

16. Chen X, Yan J, Karlsson AM. On the determination of residual stress and mechanical properties by indentation. Materials Science and Engineering A-Structural Materials Properties Microstructure and Processing, 2006, 416(1-2): 139-149.
17. Yan J, Chen X, Karlsson AM. Determining equi-biaxial residual stress and mechanical properties from the force-displacement curves of conical microindentation. Journal of Engineering Materials and Technology-Transactions of the ASME, 2007, 129(2): 200-206.
18. Yan J, Karlsson AM, Chen X. On internal cone cracks induced by conical indentation in brittle materials. Engineering Fracture Mechanics, 2007, 74(16): 2535-2546.
19. Yan J, Karlsson AM, Chen X. Determining plastic properties of a material with residual stress by using conical indentation. International Journal of Solids and Structures, 2007, 44(11-12): 3720-3737.
20. Yan J, Karlsson AM, Bartsch M, Chen X. On stresses induced in a thermal barrier coating due to indentation testing. Computational Materials Science, 2009, 44(4): 1178-1191.
21. Phadikar JK, Bogetti TA, Karlsson AM. On establishing elastic-plastic properties of a sphere by indentation testing. International Journal of Solids and Structures, 2012, 49(14): 1961-1972.
22. Phadikar JK, Bogetti TA, Kaliakin VN, Karlsson AM. Conical indentation of a viscoelastic sphere. Journal of Engineering Materials and Technology-Transactions of the ASME, 2013, 135(4): 041001.
23. Li HZ, Li SG, Wang YC. Prediction of effective thermal conductivities of woven fabric composites using unit cells at multiple length scales. Journal of Materials Research, 2011, 26(3): 384-394.
24. Li HZ, Kandare E, Li SG, Wang YC, Kandola BK, Myler P, Horrocks AR. Micromechanical finite element analyses of fire-retarded woven fabric composites at elevated temperatures using unit cells at multiple length scales. Computational Materials Science, 2012, 55: 23-33.
25. Li HZ, Kandare E, Li SG, Wang YC, Kandola BK, Myler P, Horrocks AR. Integrated thermal,

micro- and macro-mechanical modelling of post-fire flexural behaviour of flame-retarded glass/epoxy composites. Computational Materials Science, 2012, 59: 22-32.

26. Li HZ, Fan XY, Yan C. Prediction of orthotropic mechanical properties of plain weave composites with matrix voids using unit cells at multiscales. Polymer International, 2013, 62(7): 1029-1037.
27. Nazemian M, Chamani M, Baghani M. A combined experimental and numerical study of the effect of surface roughness on nanoindentation. International journal of applied mechanics, 2019, 11(7): 1950070.
28. Campbell AC, Bursikova V, Martinek J, Klapetek P. Modeling the influence of roughness on nanoindentation data using finite element analysis. International journal of mechanical sciences, 2019, 161: 105015.
29. Gao CH, Proudhon H, Liu M. Three-dimensional finite element analysis of shallow indentation of rough strain-hardening surface. Friction, 2019, 7(6): 587-602.
30. Zhou Y, Fan QB, Liu X, Wang DD, Zhu XJ. Experimental study and crystal plasticity finite element simulations of nano-indentation-induced lattice rotation and the underlying mechanism in TC6 single alpha-grain. Materials & design, 2020, 188: 108423.
31. Sneddon IN. The relation between load and penetration in the axisymmetric Boussinesq problem for a punch of arbitrary profile. International Journal of Engineering Science, 1965, 3(1): 47-57.
32. Hay JC, Bolshakov A, Pharr GM. A critical examination of the fundamental relations used in the analysis of nanoindentation data. Journal of Materials Research, 1999, 14(6): 2296-2305.

Figures

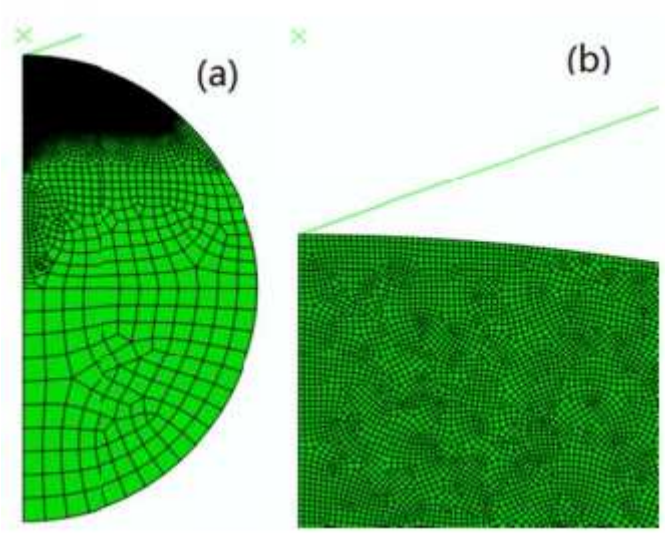

Figure 1

[See manuscript for figure legend.]

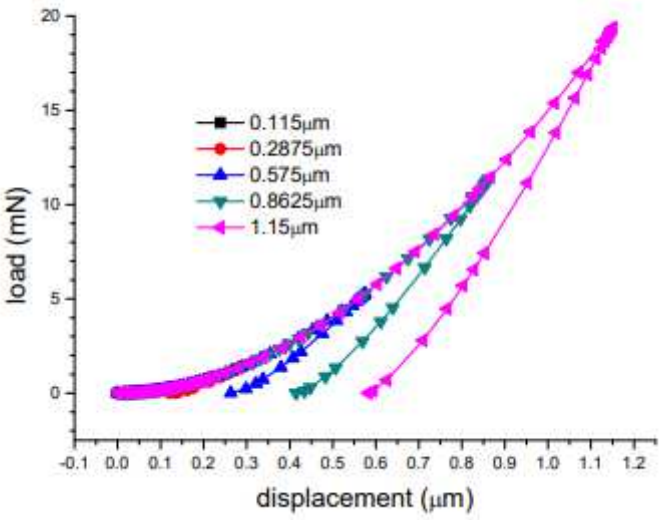

Figure 2

Loading and unloading curves for different indentation depths of / 10

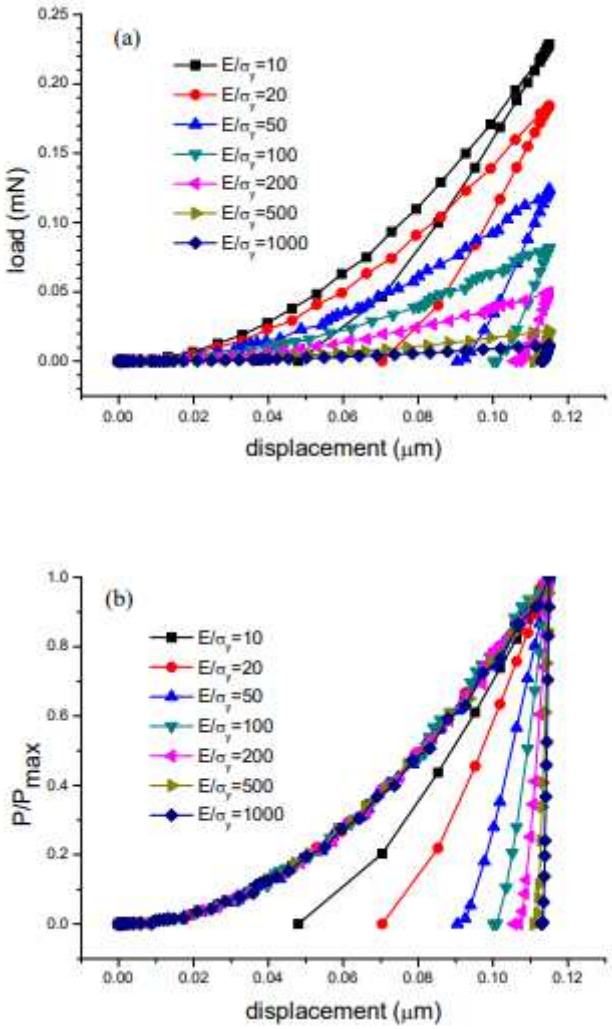

Figure 3

Loading and unloading curves for different / E y at indentation depth 0.115μm: (a) original curves, (b) curves normalized by maximum load

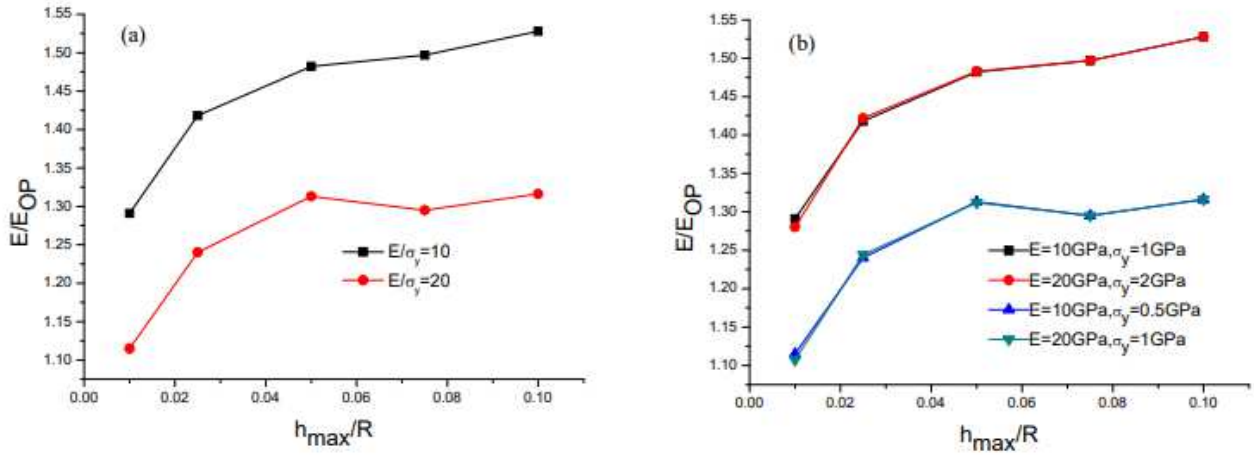

Figure 4

Normalized Young's modulus OP E E/ as a function of maximum indentation depth over microsphere radius: (a) vary y , (b) vary E

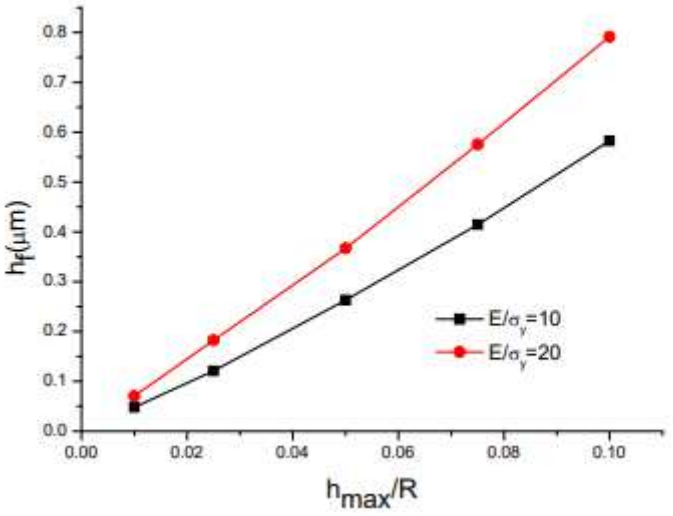

Figure 5

Final depth as a function of maximum indentation depth over microsphere radius

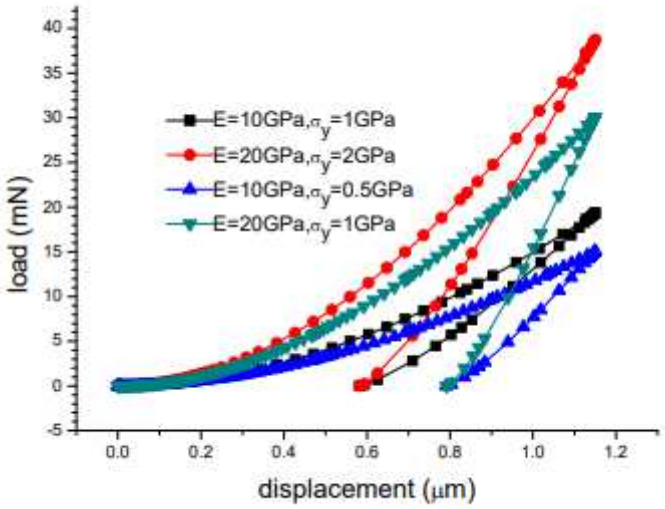

Figure 6

Loading and unloading curves for / 10 E y and / 20 E y at indentation depth 0.115μm

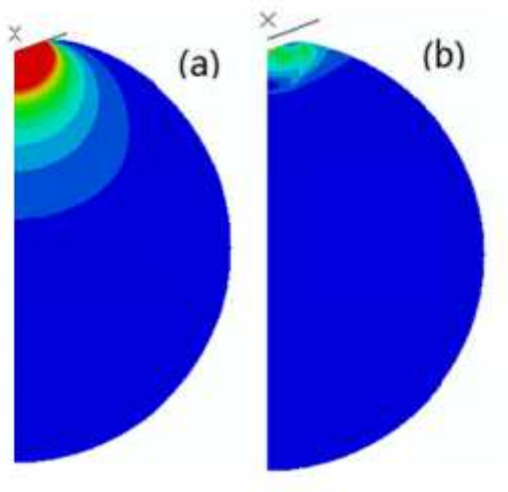

Figure 7

[See manuscript for figure legend.]